photonics

MDPI

Article

Efficiency of Photoconductive Terahertz Generation in Nitrogen-Doped Diamonds

Vitali V. Kononenko [1,*], Maxim S. Komlenok [1], Pavel A. Chizhov [1], Vladimir V. Bukin [1], Vladislava V. Bulgakova [1], Andrey A. Khomich [2], Andrey P. Bolshakov [1], Vitaly I. Konov [1] and Sergey V. Garnov [1]

[1] Prokhorov General Physics Institute of the Russian Academy of Sciences, Vavilov Street 38, 119991 Moscow, Russia; komlenok@nsc.gpi.ru (M.S.K.); pvch@kapella.gpi.ru (P.A.C.); vbkn@kapella.gpi.ru (V.V.B.); vbulgakova@kapella.gpi.ru (V.V.B.); bolshak@ran.gpi.ru (A.P.B.); vik@nsc.gpi.ru (V.I.K.); garnov@kapella.gpi.ru (S.V.G.)

[2] Kotelnikov Institute of Radio Engineering and Electronics of the Russian Academy of Sciences, 141120 Fryazino, Russia; antares-610@yandex.ru

* Correspondence: vitali.kononenko@nsc.gpi.ru

Abstract: The efficiency of the generation of terahertz radiation from nitrogen-doped (~0.1–100 ppm) diamonds was investigated. The synthetic polycrystalline and monocrystalline diamond substrates were pumped by a 400 nm femtosecond laser and tested for the photoconductive emitter operation. The dependency of the emitted THz power on the intensity of the optical excitation was measured. The nitrogen concentrations of the diamonds involved were measured from the optical absorbance, which was found to crucially depend on the synthesis technique. The observed correlation between the doping level and the level of the performance of diamond-based antennas demonstrates the prospects of doped diamond as a material for highly efficient large-aperture photoconductive antennas.

Keywords: pulse THz radiation; large-aperture photoconductive antenna; diamond; optical defects; femtosecond pumping; laser plasma and photocurrent

check for updates

Citation: Kononenko, V.; Komlenok, M.; Chizhov, P.; Bukin, V.; Bulgakova, V.; Khomich, A.; Bolshakov, A.; Konov, V.; Garnov, S. Efficiency of Photoconductive Terahertz Generation in Nitrogen-Doped Diamonds. *Photonics* **2022**, *9*, 18. https://doi.org/10.3390/photonics9010018

Received: 6 December 2021
Accepted: 27 December 2021
Published: 29 December 2021

Publisher's Note: MDPI stays neutral with regard to jurisdictional claims in published maps and institutional affiliations.

Copyright: © 2021 by the authors. Licensee MDPI, Basel, Switzerland. This article is an open access article distributed under the terms and conditions of the Creative Commons Attribution (CC BY) license (https://creativecommons.org/licenses/by/4.0/).

1. Introduction

Various techniques are used to generate THz radiation, including the acceleration of photoexcited carriers in photoconductive antennas (PCAs) [1], second-order nonlinear phenomena in electro-optical crystals (optical rectification) [2] and laser-breakdown plasmas [3]. PCAs pumped by femtosecond laser radiation are one of the most commonly used pulsed THz radiation sources [4,5]. The main features of the radiation generated by large-aperture PCAs are the low-frequency peak in the emission spectrum and the quasi-half-cycle pulse of the emitted radiation [6,7]. Currently, the study of promising substrate materials suitable for different pump lasers is of great interest for high-power large-aperture PCA devices [8–13].

One of the ways to boost the amplitude of the THz field is to increase the bias voltage applied to the PCA. Diamond has the highest dielectric strength out of all the THz-emitting substrates: its breakdown electric field was demonstrated to achieve 10 MV/cm [14]. There are additional extraordinary properties that make diamond attractive for PCA applications. Diamond is highly transparent in the THz region [15] and has already been used for THz optics [16]. Monocrystalline diamonds have a record mobility of ~4500 cm^2 V^{-1} s^{-1} at room temperature among crystalline materials [17]. Polycrystalline diamond wafers produced in a chemical vapor deposition (CVD) process are available now with diameters of over 100 mm. On the other hand, diamond is a wide-bandgap (5.46 eV) semiconductor and requires deep ultraviolet radiation for the efficient one-photon excitation of the electronic subsystem. Therefore, the first diamond PCA was pumped by an excimer laser operated at 248 nm [8]. Femtosecond UV lasers are complex systems and can hardly be used to build table-top THz sources.

Recently, nitrogen-doped diamonds were shown to be prospective candidates for THz PCAs [18]. The substitutional nitrogen evidently appeared to be an effective source of photoelectrons promoted to the conduction band by the second harmonic of a Ti:sapphire laser (400 nm). In our previous work [18], two monocrystalline CVD and HPHT (high-pressure high-temperature) diamonds were used. The nitrogen concentration of the HPHT sample was ~10 times the nitrogen concentration of the CVD sample. In this work, the nitrogen content in the diamonds varied over three orders of magnitude (~0.1–100 ppm), which allowed a detailed analysis of the effect of the nitrogen concentration on the performance of diamond PCAs to be carried out.

2. Materials and Methods

Nineteen diamond substrates of different origins with different nitrogen impurity levels were tested as PCAs. Polycrystalline and monocrystalline CVD and monocrystalline HPHT diamonds were used; they were purchased from different sellers. The typical sample size varied from 3 mm to 7 mm, and the thickness varied from 250 μm to 1570 μm. Face and edge surfaces were polished mechanically to an optical quality. Each of the assembled diamond antennas constituted the sample, with aluminum foil electrodes glued to their edges. The gap between the electrodes was limited by the substrate geometry and ranged from 0.5 to 2 mm.

The femtosecond Ti:sapphire laser system Coherent Elite Pro (800 nm fundamental wavelength, 3 mJ pulse energy, 150 fs pulse duration, 12 mm beam diameter at the $1/e^2$ level, 1 kHz repetition rate) was used for the excitation of the diamond PCAs. The experimental scheme is depicted in detail in Figure 1. The output laser beam was reduced two-fold in diameter by a telescope. Second harmonic radiation with a maximum pulse energy of 1 mJ was produced in a BBO crystal (β-barium borate, I-type, $10 \times 10 \times 0.2$ mm^3). The second harmonic pump was filtered by a cold mirror reflecting the 400 nm radiation. The energy of the second harmonic pulse was adjusted by tilting the second harmonic crystal.

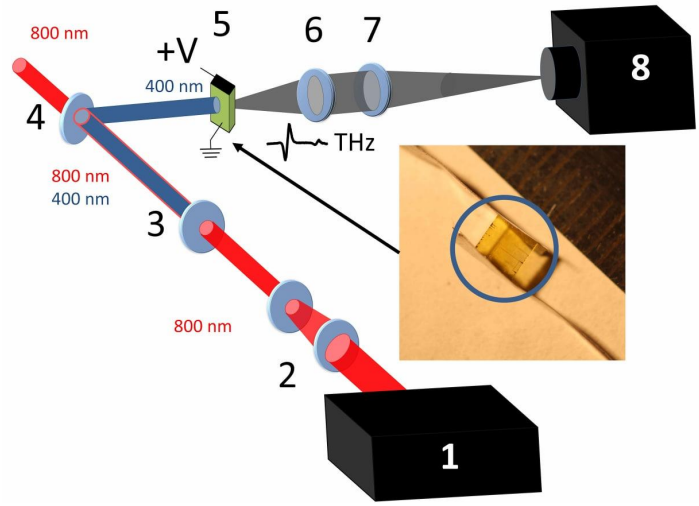


Figure 1. Experimental setup: 1—fs-laser; 2—telescope; 3—BBO crystal (SHG); 4—2nd harmonic (at 400 nm) selector; 5—diamond PCA; 6—PTFE lens (f = 6 cm); 7—PTFE lens (f = 10 cm); 8—Golay detector.

The antennas were irradiated by the central part of the unfocused pump beam with a maximum laser fluence of ~7200 μJ/cm^2. A pulsed bias voltage (up to 3 kV) with a pulse duration of ~10 ns was synchronized with the laser radiation. It should be noted that we have not achieved any THz yield with static high voltage applied to the diamond samples. THz radiation from the antennas was collected by a telescope consisting of two polytetrafluoroethylene (PTFE) lenses (50 mm diameter, 6 cm focal length and 50 mm diameter, 10 cm focal length). The power of the THz signal was measured by a Golay cell

(Tydex GC-1P, 6 mm detector aperture, 10^5 V/W illumination responsivity) with a 15 Hz modulation of the laser output.

3. Results and Discussion

3.1. Optical Properties of Nitrogen-Doped Monocrystalline HPHT and Monocrystalline and Polycrystalline CVD Diamonds

Figure 2 depicts the typical UV-visible and IR spectra of optical losses in the three types of diamonds used. The main information was deduced from the spectral data of the UV-visible range. The blue curves in Figure 2a indicate spectral decomposition in different optical loss channels, including nitrogen absorption and Rayleigh scattering. The red curve represents a sum of these individual channels of optical losses. (Band-to-band transitions were excluded from the spectral analysis.)

The absorption was approximated by two Gaussian peaks at 4.6 eV (270 nm) and 3.6 eV (345 nm) with peak widths of ∼0.4 eV and ∼0.6 eV, respectively. The visible band is assigned to the transition from the defect level of substitutional nitrogen to the conduction band, while the UV band is assigned to the transition from the valence band to the unoccupied defect level [19]. The 4.6 eV peak is the most intensive and is considered to be the most preferable in order to determine the nitrogen content level in diamonds [20]. On the whole, the intensity of the 3.6 eV peak changed in accordance with the 4.6 eV peak. While the amplitude of each peak changed over three orders of magnitude, their ratio was 2.1 ± 1.0 in our experiments.

The nitrogen level in the diamonds involved was calculated as $N_S = I_{abs}(4.6\text{ eV}) \cdot k(4.6\text{ eV})$, where $k(4.6\text{ eV}) \approx 1$ ppm/cm^{-1} is a calibration coefficient obtained in [20] using electron spin resonance (ESR) spectroscopy. In the presented set of diamond samples, the calculated content of substitutional nitrogen ranged from 10^{-1} ppm to 10^2 ppm. The HPHT samples filled this range entirely ($N_{HPHT} \approx 10^{-1}$–10^2 ppm), while the CVD samples had rather moderate concentrations of nitrogen up to $N_{CVD} < 10$ ppm because of the known difficulties of introducing nitrogen into diamond during this deposition process. IR data (Figure 2b) enabled us to estimate the N_S content level for monocrystalline diamonds only (both HPHT and CVD). The bands 1130 cm^{-1} and 1344 cm^{-1}, which are usually ascribed to the N_S center, were not detected for the relatively thin polycrystalline CVD samples that are typical for these diamonds [19]. The nitrogen contents estimated from UV-visible data and, where it was possible, from IR data differed widely (compare Figure 2a,b) but were of the same order of magnitude. Hereafter, we use N_S values calculated from the 4.6 eV absorption peak.

The samples whose spectra are depicted in Figure 2a have approximately equal nitrogen concentrations. These data clearly indicate that the magnitude of the optical losses in the visual-UV range crucially depends on the substrate origin. The polycrystalline CVD diamond substrate showed the maximum losses. The reason for this is the Rayleigh scattering that arises from subwavelength fluctuations of medium permittivity, which are the most intensive for the polycrystalline diamond. The scattering component of the absorbance was calculated as follows:

$$A_S = Sd\lambda^4, \tag{1}$$

where d is the sample thickness, λ is the wavelength and S is a scattering factor, which depends on the number of scattering centers in the medium N_{scatt}, the diameter D of such centers and the substrate refractive index n:

$$S = N_{scatt}\frac{2\pi^5}{3}D^6\left[\frac{n^2-1}{n^2+2}\right]^2. \tag{2}$$

As can be seen in Figure 2a, for the HPHT diamond, the absorption losses dominate, while the scattering is close to zero. For the monocrystalline CVD diamond, these components are rather similar. This result is not quite surprising because the CVD technique is

known to favor the formation of linear defects in the lattice. Additionally, as already mentioned, scattering is the main reason for the high optical density of the polycrystalline plates.

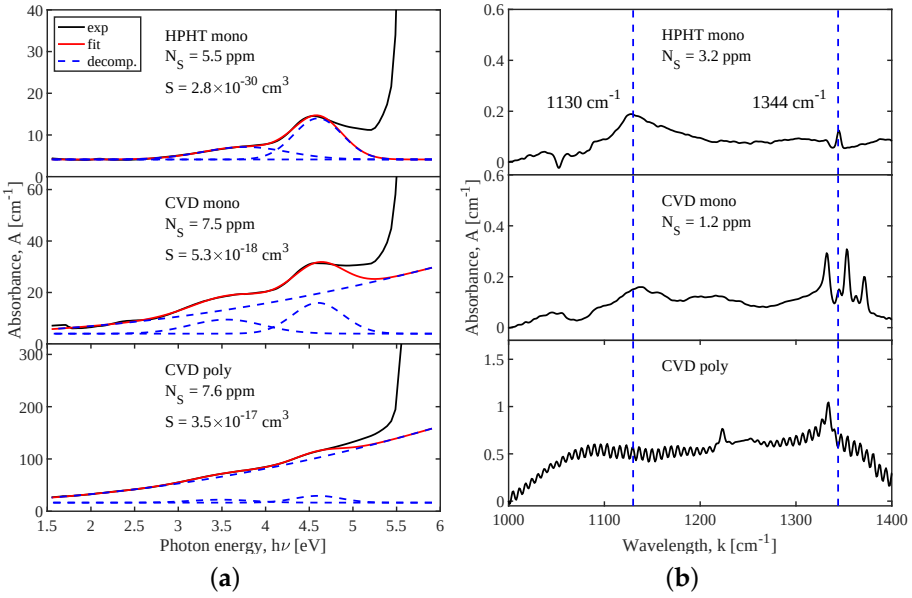


Figure 2. Optical absorption of diamond substrates of different origins in (**a**) UV-visible and (**b**) IR ranges. In UV-visible spectra, the solid red and dashed blue lines indicate spectrum decomposition and the corresponding individual channels of optical losses, including nitrogen absorption and Rayleigh scattering. In IR spectra, the blue vertical lines mark the bands characterizing substitutional nitrogen.

This conclusion was corroborated by the measurement of the diamonds' optical properties using the second harmonic of a Ti:sapphire laser. Figure 3 illustrates the dependence of the diamond absorbance per unit depth on the nitrogen concentration. The plotted data are obviously separated into three groups. Each of them exactly corresponds to the origin of the diamonds and linearly depends on the nitrogen concentration. The first group included HPHT diamonds and describes "pure" absorption losses characterized by a minimum optical density per ppm of nitrogen. The second group included CVD monocrystalline diamonds and had an absorbance per sample that was ~4 times higher than in the case of HPHT diamonds. The absorbance of the diamonds in the third group (polycrystalline diamonds) was found to be about 20 times higher.

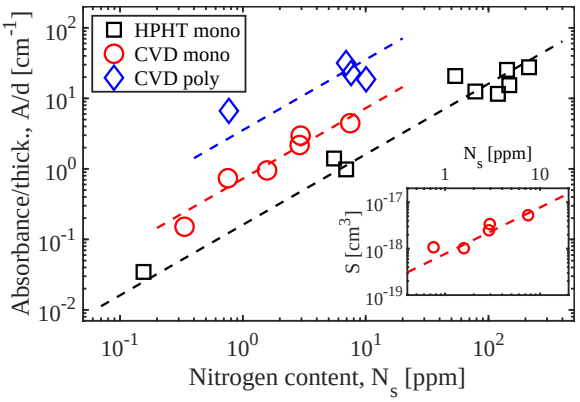


Figure 3. Dependence of diamond substrate absorbance (optical density) per unit depth on the nitrogen concentration. The measurements were performed at a pump wavelength of 400 nm. Dashed lines are linear fittings. The insert shows the optical scattering factor *S* for monocrystalline CVD diamonds (see text for details).

It is noteworthy that there is some discrepancy between the spectroscopy of monocrystalline CVD diamonds and the corresponding laser measurements. The results of the laser experiments (Figure 3) indicate that the variation of an absorbance/thickness parameter in CVD monocrystals can be completely attributed to the absorption effect. In other words, the scattering magnitude does not depend on the nitrogen level and the scattering factor S is an approximately constant value over this sample set. On the other hand, the scattering factors S calculated from spectral data with Equation (1) and depicted in the insert of Figure 3 demonstrate that optical scattering linearly increases with N_s. Therefore, at the moment, we cannot conclusively determine if the nitrogen impurity is the factor enhancing the scattering in diamonds. However, it is of interest to estimate the possible size of optical fluctuations in CVD diamonds. Using a factor $S \approx 10^{-18}$ cm^3 and a scattering center number of $N_{scatt} \approx 10^{17}$ cm^{-3} ($\sim N_S$), Equation (2) gives $D \sim 10$ nm, which is a more-or-less reasonable value in terms of the typical dislocation size.

3.2. Photoconductive THz Antennas Based on Nitrogen-Doped Monocrystalline HPHT and Monocrystalline and Polycrystalline CVD Diamonds

The dependence of the THz pulse energies on the optical pump fluence is shown in Figure 4. The fitting of the experimental data was performed using a model of THz generation that predicted the saturation of the THz field due to its interaction with a bias field [21]. According to this model, the emitted THz fluence can be written as:

$$F_{THz} = \frac{\tau E_{bias}^2}{2Z_0} \left(\frac{F_{pump}}{F_{pump} + F_{sat}^{ideal}} \right)^2, \quad (3)$$

where E_{bias} is the applied bias field, τ is the THz pulse duration, Z_0 is the free space impedance, F_{pump} is the pump fluence, and F_{sat}^{ideal} is the saturation fluence, which is the key parameter characterizing the antenna performance. In [21], this is given as

$$F_{sat}^{ideal} = \frac{h\nu(1 + n_{THz})}{e\mu Z_0(1 - R)}, \quad (4)$$

where n_{THz} is a medium refractive index in the THz range, $h\nu$ is the optical photon energy, e is the electron charge, μ is the carrier mobility, and R is the optical reflection of the substrate. We use the superscript "ideal" to emphasize that the expression for the saturation fluence is valid for non-transparent semiconductors and explicitly suggests the total surface absorption of pump radiation.

As can be seen in Figure 4, the generated THz energy is approximated satisfactorily by Equation (4): at small F_{pump} values, the emitted energy increases as the square of F_{pump}, and then saturates. In the best case, the THz power achieved a maximum of ~200 pJ with a bias field of 25 kV/cm. For an irradiated area of 2.7×1.5 mm^2, this relatively weak field provided an optical-to-THz conversion efficiency at the level of $\eta \approx 0.002\%$. The THz yield in a diamond PCA grows as the square of the applied electric field [18] and, therefore, an increase of the bias voltage up to 1 MV/cm (the breakdown electric field of diamond is 10 MV/cm [14]) is expected to scale the conversion efficiency up to ~3% and more.

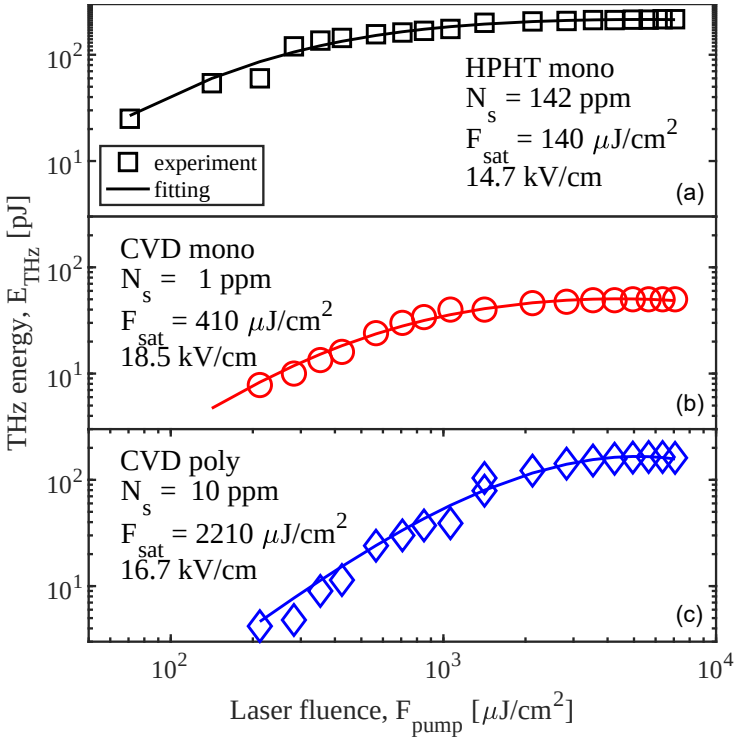


Figure 4. Experimental dependence of THz energy (dots) emitted by different diamond PCAs on the optical laser fluence: (**a**) HPHT diamond (high nitrogen level), (**b**) monocrystalline CVD diamond (low nitrogen level) and (**c**) polycrystalline CVD diamond (moderate nitrogen level). Solid lines designate curves that were fitted according to Equation (3).

The waveform of a THz pulse measured by electro-optical sampling is exemplified in Figure 5. Note that all the measured waveforms featured a clear asymmetry in the electrical field polarity and the corresponding spectra (not shown here) obtained via Fourier transform had a low-frequency maximum (0.2–0.3 THz).

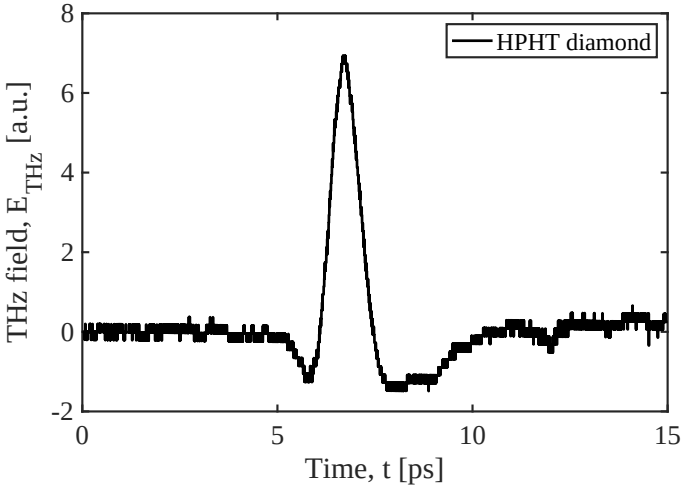


Figure 5. Waveform of THz pulse produced by HPHT diamond PCA.

The deduced saturation laser fluence is plotted in Figure 6 against the concentration of nitrogen in diamonds. The F_{sat} value is evidently correlated with the N_S content, gradually decreasing as the doping level increases. In order to model this saturation fluence behavior, a quite obvious approach was used. In Equation (4), we introduced a factor that allows only

a part of the pump pulse to be deposited in a transparent diamond. The real saturation fluence will then depend on the nitrogen concentration in the substrate:

$$F_{sat} = \frac{F_{sat}^{ideal}}{1 - exp(-\alpha d)}, \quad (5)$$

where α is the nitrogen-doped diamond absorption and d is the sample thickness. As the sample thickness varied over a wide range (from 250 μm to 1570 μm), Figure 6 contains two marginal curves calculated with the marginal thicknesses from Equation (5). The absorption value was taken from the laser experiment (Figure 3). The minimum experimental saturation fluence of ~40 μJ/cm^2, demonstrated by the ~200 ppm HPHT diamond, was taken as an "ideal" F_{sat}. This is, to the best of our knowledge, the lowest saturation fluence under 400 nm pumping.

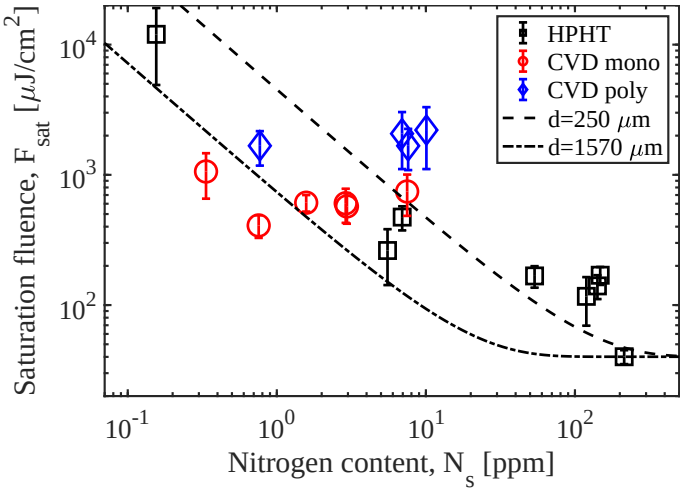


Figure 6. Dependence of saturation laser fluence on nitrogen concentration for tested diamond emitters. The lines indicate theoretical estimations of PCA performance for 250-μm-thick and 1570-μm-thick substrates (see text for details).

Taken as a whole, the data in Figure 6 support the theoretical model. The best ($F_{sat} \approx 40$ μJ/cm^2) and the worst ($F_{sat} \approx 12{,}000$ μJ/cm^2) performances were demonstrated by HPHT diamonds with the maximum and minimum nitrogen concentrations, respectively. Despite the remarkable data spreading, the major part of the experimental points lies inside the predicted channel. Only three specific groups appear to be excluded from this channel.

The first group includes the HPHT high-doped diamonds, which are characterized by a saturation fluence that is 70%–100% above the theoretical estimation. The possible physical mechanism of the emission weakening here is a decrease in the mobility of carriers in high-nitrogen-impurity crystals. The second group covers the polycrystalline CVD diamonds with $N_S \approx 10$ ppm, whose saturation fluence exceeds approximately twice the theoretical limit. This can be caused, as in the first case, by damped electron mobility. The second important factor that obviously deteriorated the efficiency of the optical-to-THz conversion is just the strong optical scattering. In polycrystalline substrates, the backward and wide-angle scattering results in a remarkable non-absorptive attenuation of the pumping radiation that, in turn, leads to a diminished number of photocarriers and photocurrent-generating THz waves. In contrast, the performance demonstrated by the third group—two monocrystalline CVD diamonds—was about twice as good as the theoretical predictions. The mechanism of these efficiency spikes is currently unclear. Supposedly, this might be achieved at the expense of the laser excitation of other color centers in addition to the substitutional nitrogen.

On the whole, the diamonds behaved rather predictably in the THz generation experiments. Meanwhile, the F_{sat} value calculated in this work for a set of 19 substrates revealed that a diamond PCA's performance can vary by one order of magnitude with an approximately constant level of nitrogen. Future work, in order to achieve precise control of the THz generation efficiency, should explore the exact reasons for this dispersion and refine the techniques of diamond synthesis and doping.

4. Conclusions

In conclusion, this work investigated terahertz generation in PCAs based on nitrogen-doped diamonds and pumped by the second harmonic of a Ti:sapphire laser. The doping level was demonstrated to precisely govern the optical absorption in high-quality HPHT and CVD diamond substrates. Consequently, the tight correlation between the doping level and the magnitude of the saturation fluence in diamond PCAs arises. The efficiency of doping as a tool for controlling the performance of diamond emitters was proven: depending on the nitrogen level, the saturation fluence of diamond PCAs ranged from very high ($\sim$12,000 $\mu J/cm^2$) to quite low ($\sim$40 $\mu J/cm^2$) for dielectric materials. The current yield of THz radiation from diamond PCA is about $\sim$0.2 nJ, while the reported emission level for a GaAs large aperture PCA (35×35 mm^2, 10.7 kV/cm) achieved $\sim$800 nJ [22]. Diamond-based antennas of comparable size are expected to emit a comparable power level. Moreover, this level can be significantly increased with increasing the applied electric field. Future work will focus on a necessity to form closely located buried electrodes in diamond bulk to provide the high bias field in a diamond PCA. These data and estimations corroborate the potential of doped diamond to be used as a material for extremely biased and efficient large-aperture photoconductive antennas.

Author Contributions: Conceptualization, V.V.K. and M.S.K.; methodology, V.V.B. (Vladimir V. Bukin); validation, V.V.B. (Vladimir V. Bukin); formal analysis, V.V.K. and P.A.C.; sample preparation, A.P.B., M.S.K. and V.V.K.; investigation, V.V.K., M.S.K., P.A.C., V.V.B. (Vladislava V. Bulgakova) and A.A.K.; data curation, V.V.K. and P.A.C.; writing—original draft preparation, V.V.K. and M.S.K.; writing—review and editing, P.A.C. and V.V.B. (Vladimir V. Bukin); supervision, V.I.K. and S.V.G.; project administration, V.V.B. (Vladimir V. Bukin) and S.V.G. All authors have read and agreed to the published version of the manuscript.

Funding: This research was funded by Ministry of Science and Higher Education of the Russian Federation, grant number 075-15-2020-790.

Institutional Review Board Statement: Not applicable.

Informed Consent Statement: Not applicable

Data Availability Statement: The authors confirm that the data supporting the findings of this study are available within the article

Conflicts of Interest: The authors declare no conflict of interest.

Abbreviations

The following abbreviations are used in this manuscript:

PCA	photoconductive antenna
HPHT	high pressure - high temperature
CVD	chemical vapor deposition
PTFE	polytetrafluoroethylene
BBO	β-barium borate

References

1. Lee, C.H. Picosecond optoelectronic switching in GaAs. *Appl. Phys. Lett.* **1977**, *30*, 84–86. [CrossRef]
2. Yang, K.; Richards, P.; Shen, Y. Generation of far-infrared radiation by picosecond light pulses in LiNbO3. *Appl. Phys. Lett.* **1971**, *19*, 320–323. [CrossRef]

3. Oh, T.; Yoo, Y.; You, Y.; Kim, K. Generation of strong terahertz fields exceeding 8 MV/cm at 1 kHz and real-time beam profiling. *Appl. Phys. Lett.* **2014**, *105*, 041103. [CrossRef]
4. Fattinger, C.; Grischkowsky, D. Terahertz beams. *Appl. Phys. Lett.* **1989**, *54*, 490–492. [CrossRef]
5. Burford, N.M.; El-Shenawee, M.O. Review of terahertz photoconductive antenna technology. *Opt. Eng.* **2017**, *56*, 010901. [CrossRef]
6. Hafez, H.; Chai, X.; Ibrahim, A.; Mondal, S.; Férachou, D.; Ropagnol, X.; Ozaki, T. Intense terahertz radiation and their applications. *J. Opt.* **2016**, *18*, 093004. [CrossRef]
7. Chai, X.; Ropagnol, X.; Ovchinnikov, A.; Chefonov, O.; Ushakov, A.; Garcia-Rosas, C.; Isgandarov, E.; Agranat, M.; Ozaki, T.; Savel'ev, A. Observation of crossover from intraband to interband nonlinear terahertz optics. *Opt. Lett.* **2018**, *43*, 5463–5466. [CrossRef] [PubMed]
8. Yoneda, H.; Tokuyama, K.; Ueda, K.; Yamamoto, H.; Baba, K. High-power terahertz radiation emitter with a diamond photoconductive switch array. *Appl. Opt.* **2001**, *40*, 6733–6736. [CrossRef]
9. Imafuji, O.; Singh, B.P.; Hirose, Y.; Fukushima, Y.; Takigawa, S. High power subterahertz electromagnetic wave radiation from GaN photoconductive switch. *Appl. Phys. Lett.* **2007**, *91*, 071112. [CrossRef]
10. Ropagnol, X.; Morandotti, R.; Ozaki, T.; Reid, M. Toward high-power terahertz emitters using large aperture ZnSe photoconductive antennas. *IEEE Photonics J.* **2011**, *3*, 174–186. [CrossRef]
11. Ropagnol, X.; Bouvier, M.; Reid, M.; Ozaki, T. Improvement in thermal barriers to intense terahertz generation from photoconductive antennas. *J. Appl. Phys.* **2014**, *116*, 043107. [CrossRef]
12. Ropagnol, X.; Kovács, Z.; Gilicze, B.; Zhuldybina, M.; Blanchard, F.; Garcia-Rosas, C.; Szatmári, S.; Földes, I.; Ozaki, T. Intense sub-terahertz radiation from wide-bandgap semiconductor based large-aperture photoconductive antennas pumped by UV lasers. *New J. Phys.* **2019**, *21*, 113042. [CrossRef]
13. Bulgakova, V.; Ushakov, A.A.; Chizhov, P.A.; Yudin, N.; Zinovev, M.; Podzyvalov, S.; Dolmatov, T.; Bukin, V.; Garnov, S. Terahertz generation by means of ZnGeP2 large aperture photoconductive antenna. *Opt. Eng.* **2021**, *60*, 082015. [CrossRef]
14. Yoneda, H.; Ueda, K.I.; Aikawa, Y.; Baba, K.; Shohata, N. Photoconductive properties of chemical vapor deposited diamond switch under high electric field strength. *Appl. Phys. Lett.* **1995**, *66*, 460–462. [CrossRef]
15. Kubarev, V. Optical properties of CVD-diamond in terahertz and infrared ranges. *Nucl. Instrum. Methods Phys. Res. Sect. A Accel. Spectrom. Detect. Assoc. Equip.* **2009**, *603*, 22–24. [CrossRef]
16. Komlenok, M.; Kononenko, T.; Sovyk, D.; Pavelyev, V.; Knyazev, B.; Ashkinazi, E.; Reshetnikov, A.; Komandin, G.; Pashinin, V.; Ralchenko, V.; et al. Diamond diffractive lens with a continuous profile for powerful terahertz radiation. *Opt. Lett.* **2021**, *46*, 340–343. [CrossRef]
17. Isberg, J.; Hammersberg, J.; Johansson, E.; Wikström, T.; Twitchen, D.J.; Whitehead, A.J.; Coe, S.E.; Scarsbrook, G.A. High carrier mobility in single-crystal plasma-deposited diamond. *Science* **2002**, *297*, 1670–1672. [CrossRef] [PubMed]
18. Chizhov, P.A.; Komlenok, M.S.; Kononenko, V.V.; Bukin, V.V.; Ushakov, A.A.; Bulgakova, V.V.; Khomich, A.A.; Bolshakov, A.P.; Konov, V.I.; Garnov, S.V. Photoconductive terahertz generation in nitrogen-doped single-crystal diamond. *Opt. Lett.* **2022**, *47*, 86–89. [CrossRef]
19. Iakoubovskii, K.; Adriaenssens, G. Optical transitions at the substitutional nitrogen centre in diamond. *J. Phys. Condens. Matter* **2000**, *12*, L77. [CrossRef]
20. Nistor, S.V.; Stefan, M.; Ralchenko, V.; Khomich, A.; Schoemaker, D. Nitrogen and hydrogen in thick diamond films grown by microwave plasma enhanced chemical vapor deposition at variable H2 flow rates. *J. Appl. Phys.* **2000**, *87*, 8741–8746. [CrossRef]
21. Benicewicz, P.; Roberts, J.; Taylor, A. Scaling of terahertz radiation from large-aperture biased photoconductors. *JOSA B* **1994**, *11*, 2533–2546. [CrossRef]
22. You, D.; Jones, R.; Bucksbaum, P.; Dykaar, D. Generation of high-power sub-single-cycle 500-fs electromagnetic pulses. *Opt. Lett.* **1993**, *18*, 290–292. [CrossRef] [PubMed]